Sangeeta K. Siri and Mrityunjaya V. Latte*

Universal Liver Extraction Algorithm: An Improved Chan-Vese Model

https://doi.org/10.1515/jisys-2017-0362
Received July 23, 2017; previously published online January 30, 2018.

Abstract: Liver segmentation is important to speed up liver disease diagnosis. It is also useful for detection, recognition, and measurement of objects in liver images. Sufficient work has been carried out until now, but common methodology for segmenting liver image from CT scan, MRI scan, PET scan, etc., is not available. The proposed methodology is an effort toward developing a general algorithm to segment liver image from abdominal computerized tomography (CT) scan and magnetic resonance imaging (MRI) scan images. In the proposed algorithm, pixel intensity range of the liver portion is obtained by cropping a random section of the liver. Using its histogram, threshold values are calculated. Further, threshold-based segmentation is performed, which separates liver from abdominal CT scan image/abdominal MRI scan image. Noise in the liver image is reduced using median filter, and the quality of the image is improved by sigmoidal function. The image is then converted into binary image. The Chan-Vese (C-V) model demands an initial contour, which evolves outward. A novel algorithm is proposed to identify the initial contour inside the liver without user intervention. This initial contour propagates outward and continues until the boundary of the liver is identified accurately. This process terminates by itself when the entire boundary of the liver is detected. The method has been validated on CT images and MRI images. Results on the variety of images are compared with existing algorithms, which reveal its robustness, effectiveness, and efficiency.

Keywords: Liver segmentation, Chan–Vese model, histogram-based threshold segmentation, computerized tomography, magnetic resonance image.

1 Introduction

Segmentation is an action by which image is fragmented into meaningful non-overlapping structures, which have the same attributes like range, color, texture, size, shape, width, height, and intensity [18]. The liver is a largest internal organ as well as a gland, which is responsible for hundreds of chemical actions that the human body needs. The liver is an organ, which is affected by diseases rapidly because of its microscopic anatomy and rich biochemical environment. Thus, liver segmentation is of high priority to plan a surgery or chemotherapy pump placement or disease diagnosis [16]. So extracting the liver from computerized tomography (CT) scan image or magnetic resonance imaging (MRI) scan image will be of prime importance. Considerable work has been done in extracting the liver from CT or MRI image. The existing segmentation algorithms are optimized for categorized images for CT scan, MRI scan and a few on positron emission tomography (PET) scan. Hence, authors opine that there is a necessity of developing an algorithm to obtain accurate and consistent results for all kinds of images. A reliable and accurate segmentation algorithm is not yet achieved due to (a) the neighboring organs of the liver like kidneys, heart, stomach, etc., having the same intensity level. (b) There is no definite shape, weight, size, volume, or texture for the liver. All these

^{*}Corresponding author: Mrityunjaya V. Latte, JSS Academy of Technical Education, Bengaluru, India, e-mail: mvlatte@rediffmail.com

Sangeeta K. Siri: Department of Electronics and Communication Engineering, Sapthagiri College of Engineering, Bengaluru, India

parameters are subjective. (c) The edges are weak. (d) The presence of artifacts in the MRI images or CT scan images.

The liver segmentation algorithm extracts the liver from the scan image, which facilitates the measurement of liver parameters like area and volume, which are crucial parameters in liver transplantation. It also helps in virtual surgery simulation, speeding up of the disease diagnosis. Manual extraction of the liver image from the abdominal scan highly depends on the skill and proficiency of the technician, which may disrupt the result. Meanwhile, manual segmentation is also time consuming.

The liver and its neighboring organs have the same intensity levels, and due to the presence of noise in the scanned images, it is difficult to find a threshold value required to separate the liver from its neighboring organs. The objectives of the proposed algorithm are (1) to reduce user interaction; (2) to design segmentation algorithm, which provides accurate and consistent results for all kinds of images and all types of modalities.

2 Related Work

Chen et al. [2] designed the liver segmentation algorithm in which the Gaussian function is used to find the liver likelihood image from the CT scan images and obtained the liver boundary using the Chan-Vese (C-V) model. They used morphological operation to improve the results. Song et al. [19] proposed an automatic liver boundary marking method, which is based on an adaptive fast marching method (FMM). The liver image is separated from the CT scan by manually fixing the pixel intensity between 50 and 200. The median filter is applied to reduce noise, and the liver image is enhanced by sigmoidal function. In this method, the image is converted into binary, and FMM is applied to find the liver boundary accurately. Wu et al. [20] developed a novel method for the automatic delineation of the liver on CT volume images using supervoxel-based graph cuts. This method integrates histogram-based adaptive thresholding, simple linear iterative clustering (SLIC) and graph cut algorithm. Moghbel et al. [11] proposed the random walker-based framework. In this, the liver dome is automatically detected based on the location of the right lung lobe and rib caged area. The liver is extracted utilizing the random walker method. Ding et al. [3] introduced a multi-atlas segmentation approach with local decision fusion for fast automated liver (with/without abnormality) segmentation on computational tomography angiography (CTA). Zheng et al. [22] designed a feature-learning-based random walk method for liver segmentation using CT images. Four texture features are extracted and then classified to determine the probability corresponding to the test images. In this, seed points on the original test image are automatically selected. Peng et al. [13] designed a novel multiregionappearance-based approach with graph cuts to delineate the liver surface, and a geodesic distance-based appearance selection scheme is introduced to utilize proper appearance constraint for each sub-region. Platero et al. [14] proposed a new approach to segment the liver from CT scan, which is a combination of low-level operations, an affine probabilistic atlas and a multiatlas-based segmentation. Salman et al. [17] presented a novel fully automatic algorithm for 3D liver segmentation in clinical 3D CT images based on Mahalanobis distance cost function using an active shape model implemented on MICCAI-SLiver07 achieving accurate results. Lu et al. [9] developed liver segmentation using the three-dimensional (3D)-convolutional neural network, and accuracy of initial segmentation is increased with graph cut algorithm and the previously learned probability map. Li et al. [8] developed a technique to detect the liver surface, which includes construction of a statistical shape model using the principal component analysis. The Euclidean distance transformation is used to obtain a coarse position in a source image. An accurate detection of the liver is obtained using the deformable graph cut method. Zheng et al. [4] designed a tree-like multiphase level set algorithm for segmentation, based on the C-V model to detect objects in an image. The algorithm is effective for images, which have sub-objects in the region. Pramod Kumar et al. [15] proposed an automatic segmentation algorithm to fragment the lung parenchyma, which is the integration of 2D optimal threshold selection and 2D reconstruction. Further segmentation results are enhanced by the improved chain code and Bresenham pixel interconnection.

Basic Chan-Vese Model

All the classical snakes and active contour models depend on the image gradient to stop the curve evolution, so these models can detect only the objects with edges defined by a gradient [1, 12, 21]. In biomedical images, the edges are fragile, and the image is noisy. Hence, the stopping function is never zero on the edges, and the curve evolution may pass through the boundary. Chan and Vese [1] designed a new active contour model for image segmentation based on region instead of gradient, which is called the C-V model. In this section, the original C-V approach [1] is summarized for reader convenience.

Let I(x) be the brightness function of the input image. The image is defined over a 2D area, denoted by R. It is assumed that the image contains objects and background, which have constant brightness, denoted by B_{\perp} and B_{\perp} , respectively. Let C represent the closed curve in the image that separates the objects and background. In the C-V model [1], the following energy function is minimized:

$$f(B_o, B_b, C) = \mu * \text{Length}(C) + \lambda * \text{Area}(\text{inside}(C)) + \lambda_o \int_{\text{inside}C} (I(x) - B_o)^2 dx + \lambda_b \int_{\text{outside}C} (I(x) - B_b)^2 dx$$
(1)

where λ , λ_b , λ_a , μ are parameters of suitably chosen values and practically set greater than or equal to zero. Equation (1) can be minimized by taking the function $\phi(x)$, $x \in \Re$, introduced by a value greater than 0 inside the objects, less than 0 outside the objects, and equal to zero on the boundaries. Using the Heaviside function, it is defined by

$$H(z) = \{1 \text{ if } z > = 0\} \text{ and } H(z) = \{0 \text{ if } z < 0\}$$
 (2)

Using equation (2), we can write equation (1) as

$$f(B_o, B_b, \phi) = \mu \int_{\Re} (|\nabla H(\phi)|) |dx + \lambda \int_{\Re} (H(\phi)) dx + \lambda_o$$
$$\int_{\Re} (I - B_o)^2 H(\phi) dx + \lambda_b \int_{\Re} (I - B_b)^2 (1 - H(\phi)) dx$$
(3)

Keeping ϕ and minimizing the value of $f(B_o, B_h, \phi)$ with respect to the constants B_o, B_h , we can take following expression for B_o , B_h

$$B_o(\phi) = \frac{\int_{\Re} IH(x)dx}{\int_{\Re} H(x)dx} \tag{4}$$

$$B_{b}(\phi) = \frac{\int_{\Re} I(1 - H(x)) dx}{\int_{\Re} (1 - H(x)) dx}$$
 (5)

It can be easily seen that the values of $B_o(\phi)$ and $B_b(\phi)$ have the meaning of average brightness of the original image over the areas that are regarded as objects ($\phi \ge 0$) and background ($\phi < 0$), respectively, in the image segmentation. Keeping B_o and B_h fixed and minimizing $f(B_o, B_h, \phi)$ with respect to ϕ , the associated Euler-Langrange equation may be obtained and takes the form of

$$\delta(\phi) * \left[\mu \operatorname{div} \left(\frac{\nabla \phi}{|\nabla \phi|} \right) - \lambda - \lambda_o (I - B_o)^2 - \lambda_b (I - B_b)^2 \right] = 0 \quad \text{in } \Re$$
 (6)

For practical computation, the author introduced the regularization version of *H* and its derivation as follows:

$$H_{\varepsilon}(z) = \frac{1}{2} \left(1 + \frac{2}{\pi} \arctan\left(\frac{z}{\varepsilon}\right) \right)$$
 ε is suitably chosen value (7)

$$\delta(z) = H'_{\varepsilon} = \frac{1}{\pi} * \frac{\varepsilon}{\varepsilon^2 + z^2} \quad \varepsilon \text{ is suitably chosen value}$$
 (8)

Introducing $\phi(T, x)$ by parameterizing the descent direction by time $T \ge 0$ and taking $\phi(0, x) = \phi(x)$ (chosen initial contour), a system is obtained for solving ϕ iteratively that can be written in the form of

$$\frac{d\phi}{dt} = \delta_{\varepsilon}(\phi) \left(\mu \operatorname{div} \left(\frac{\nabla \phi}{|\nabla \phi|} \right) - \lambda - \lambda_{o} (I - B_{o})^{2} - \lambda_{b} (I - B_{b})^{2} \right) \text{ in } \Re$$
(9)

$$\phi(0, x) = \phi_{\alpha}(x) \text{ in } \Re \text{ and } = 0 \text{ on } \delta \Re$$
 (10)

where \vec{n} denotes the exterior normal to the boundary $\delta\Re$ of \Re , and $\frac{\partial \varphi}{\partial \vec{n}}$ denotes the normal derivation φ at the boundary. $\varphi_o(x)$ is a signed distance function, and the initial contour is defined as a curve satisfying $\varphi_o(x) = 0$.

4 Algorithm Used for an Automatic Initialization

The C–V model requires an initialization window. A novel algorithm is developed to design the initialization window inside the liver, which develops outward until it reaches the liver periphery. The algorithm steps are as follows:

- Step 1: Find the centroid of the liver as (x_{cent}, y_{cent}) , take $\bar{x} = 4$, $\bar{y} = 4$ and the area of the liver.
- Step 2: Take the initial contour as $(y_{cent}, y_{cent} + \overline{y}; x_{cent}, x_{cent} + \overline{x})$.
- Step 3: Initialize stop = 0.
- Step 4: Generate a signed distance function (SDF) from the initial contour.
- Step 5: Get the narrow band of the initial contour and find the interior and exterior mean.
- Step 6: Find the value of the force using the equation.

$$F = (P - U)^{2} + (P - V)^{2}$$
(11)

here U = the interior mean, V = the exterior mean, and P = the pixel coordinate value.

Step 7: If the force is less than 1, then increment the \bar{x} , \bar{y} value and go to step 4, or else, stop, and take $(y_{cent}, y_{cent}, x_{cent}, x_{c$

5 Methodology

The proposed algorithm has four steps in liver segmentation: (a) pre-processing; (b) finding the pixel intensity range of the liver, i.e. finding T_{\min} and T_{\max} to remove the neighboring organs of the liver like the kidney, stomach, spleen, and ribs; (c) design of an initialization contour so that the curve evolution starts; (d) applying the C–V model to mark a boundary for the liver.

- (a) **Pre-processing:** The abdominal CT/MRI scan image is with a 1019×682 DICOM color format. First, convert the CT/MRI scan image into a grayscale image of size 512×512 .
- **(b) Finding the pixel intensity range in the liver:** The liver pixel intensity levels vary from patient to patient, as well as they vary throughout the liver area. Cropping the liver image is done to study the behavior of the pixel intensity variation. This is done randomly without having prior knowledge of the liver image. The pixel intensity also depends upon the disease associated with the liver. Hence, getting the liver pixel intensity range is a complicated task. In the proposed algorithm, the liver part is cropped, and a histogram is obtained. The pixel intensity within the liver varies from 0 to 255. The exact range for a particular patient's liver is obtained from the histogram of the cropped liver section. From the histogram, the pixel intensity range

for a particular patient is computed. In the computed range, the maximum pixel intensity level (T_{\max}) and the minimum pixel intensity level (T_{\min}) are obtained. Using T_{\min} and T_{\max} , a threshold-based segmentation is performed.

$$I = \begin{pmatrix} I & \text{if} & T_{\min} \le I \le T_{\max} \\ 0 & \text{if} & \text{Otherwise} \end{pmatrix}$$
 (12)

This separates the liver from its neighboring organs. The noise in the image is reduced by applying a median filter. Enhancement of the image is done by sigmoidal function. Then the image is converted into binary.

- **(c) Initialization contour:** An initialization contour is automatically chosen using the centroid of the liver, and a force greater than 1 is obtained.
- **(d) Chan–Vese model:** The initialization contour, binary image, and area of the liver are inputs to the C–V model. The initialization contour progresses outward and stops at the periphery of the liver. This model is used to find the liver outline accurately for the CT scan and MRI scan images.

The image is cropped to the required size from a reference point identified randomly. The histogram of the cropped image is obtained. The minimum and maximum pixel values of the histogram are represented as the minimum threshold T_{\min} and maximum threshold T_{\max} , respectively. The threshold-based segmentation is applied on the scanned image to retain only the liver image and remove the neighboring organs. Further, the liver image is converted into a binary image. In the next step, the initialization contour is identified inside the liver section without user intervention, which grows outward using the C–V model until the complete boundary of the liver is obtained. The flowchart shown in Figure 1 depicts the complete process of identifying the contour of the liver image.

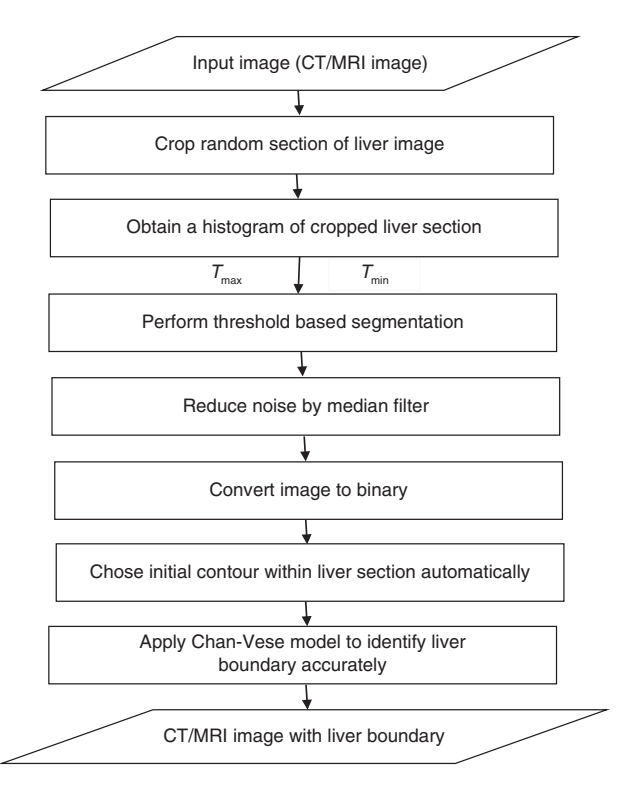


Figure 1: Process of Proposed Method.

6 Liver Segmentation Evaluation Metrics

Image segmentation plays an imperative role in a wide range of applications. Evaluating the competence of the segmentation algorithm for a given application is obligatory both to allow the proper selection of the segmentation algorithm as well as to fine tune their parameters for the finest performance. The experimental disagreement method is based on the availability of the reference segmented image, also named the ground truth image. The discrepancy between a segmented image and a ground truth image is used to gauge the algorithm performance. Both images (ground truth and segmented images) are acquired from the same input image [21]. The following error measures are adopted to assess the proposed method:

6.1 Volumetric Overlap Error (VOE)

The VOE between two sets of voxel S_{SEG} and S_{GT} is given in percent and defined as (1 – Jaccardcoefficient), where the Jaccard coefficient is the ratio between the intersection and the union of S_{SEG} and S_{GT} . S_{GT} is the ground truth image or reference image obtained by manual segmentation under the supervision of an expert, and S_{GFG} is the segmented image. The volumetric overlap error is 0% for perfect segmentation and 100% if the segmentation and ground truth image do not overlap [10]. The volumetric overlap error lies between 0% and 100%. This method is one of the most popular methods to evaluate segmentation accuracy and is selected for that reason [5, 10].

6.2 Relative Volume Difference (RVD)

The RVD between the two sets S_{SEG} and S_{GT} is given in percent and defined as $100(|S_{\text{SEG}} - S_{GT}|)/|S_{GT}|$, with $S_{\text{SEG}} = S_{GT} = S_{GT}$ as the segmented image and S_{GT} as the ground truth image [5, 10]. A value of 0 means that both volumes are identical or both images overlap with each other [5].

6.3 Average Symmetric Surface Distance (ASSD)

The ASSD is given in millimeters and based on the surface voxels of two segmentations of S_{SEG} and S_{GT} . Surface voxels are defined by having at least one non-object voxel within their 18 neighborhood [10]. For each surface voxel of S_{SFG} , the Euclidean distance to the closest surface voxel of S_{GT} is calculated using the approximate nearest neighbor technique and stored [10]. In order to provide the symmetry, the same process is applied from the surface voxels of S_{CT} to S_{SEG} . The ASSD is then defined as the average of all stored distances, which is zero for perfect segmentation algorithm.

Let S(seg) denote the set of surface voxel of segmentation. The short distance of a voxel to S(seg) is defined as:

$$d(V, S(seg)) = \min_{S_{see} \in S(seg)} (|V - S(seg)|)$$
(13)

where the |. | operation denotes the Euclidean distance. The average symmetric surface is then given by

$$ASSG(S_{SEG}, S_{GT}) = \frac{1}{|S_{SEG}| + |S_{GT}|} * (\Sigma_{S_{SEG} \in S(SEG)} d(S_{SEG}, S(SG)) + \Sigma_{S_{GT} \in S(GT)} d(S_{GT}, S(SEG))$$
(14)

6.4 Maximum Symmetric Surface Distance (MSSD)

The MSSD is given in millimeter and determined similar to the previous metric. It is also called the Haudorff distance [10]. The differences between both sets of surface voxels are determined using Euclidean distances,

and the maximum value yields the maximum symmetric surface distance. For perfect segmentation, this distance is 0.

$$MSSD(S_{SEG}, S_{GT}) = \max[\max \Sigma_{S_{cro} \in S(SEG)} d(S_{SEG}, S(SEG)), \max \Sigma_{S_{cro} \in S(GT)} d(S_{GT}, S_{SEG})]$$
(15)

This metric is sensitive to boundary and returns the true maximum error.

7 Experimental Results and Discussions

The experimental dataset consists of CT scan images and MRI scan images of 50 patients, which are provided by M/S CT scan Centre, Hubli, Karnataka, India. Each slice of CT scan is a 1019×682-size color image.

The results of the CT scan and MRI scan images are shown in Figures 2 and 3, respectively. The original CT scan and MRI scan images are shown in Figures 2A and 3A, respectively. Cropping a random section of the liver in the CT scan and MRI scan images are shown in Figures 2B and 3B, respectively. The histograms of a cropped liver section in the CT scan and MRI scan images are shown in Figures 2C and 3C, respectively. The results of the histogram-based liver separation from its neighboring organs in CT scan and MRI scan images are shown in Figures 2D and 3D, respectively. The liver boundary markings in CT scan and MRI scan images are shown in Figures 2E and 3E, respectively. The ground truth images of the CT scan and MRI scan images are shown in Figures 2F and 3F, respectively.

The experimental results of three CT scan images and three MRI scan images are shown in Figures 4 and 5, respectively; column A shows the original CT scan images and MRI scan images, column B shows the liver boundary markings in the CT scan images and MRI scan images, and column C shows the ground truth images of the CT scan images and MRI scan images.

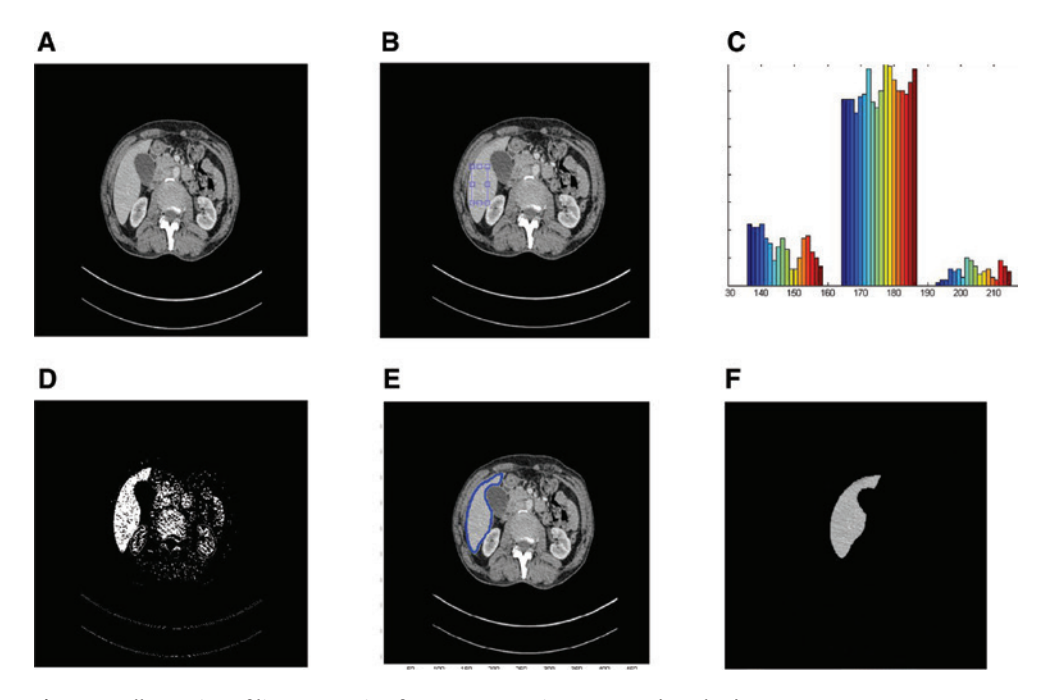


Figure 2: Illustration of liver extraction from CT scan using proposed method. (A) Original CT Scan Image. (B) Cropping Random Section of Liver. (C) Histogram of Cropped Liver Section. (D) Result of Histogram-Based Segmentation. (E) Liver Boundary in CT Scan. (F) Ground Truth Image.

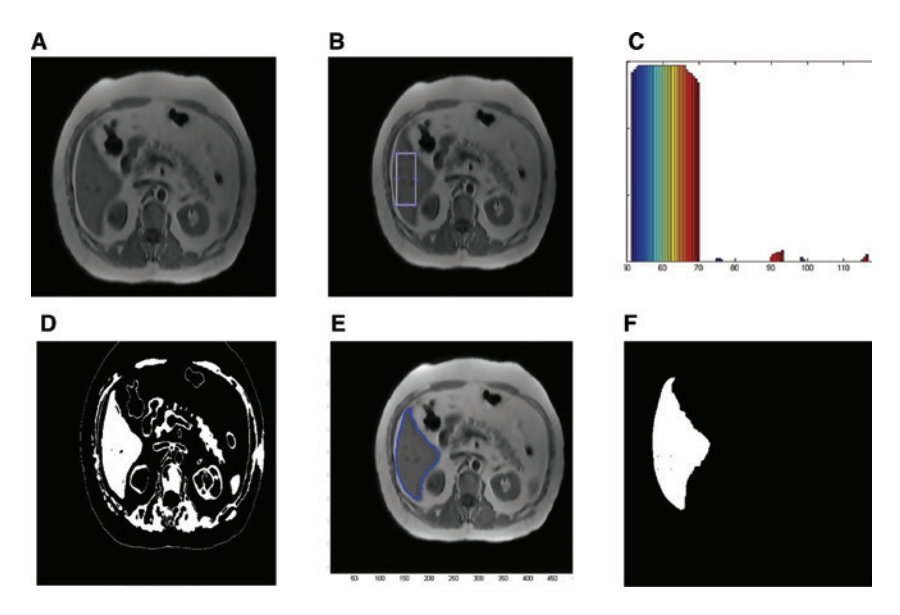


Figure 3: Illustration of liver extraction from MRI scan using proposed method.
(A) Original MRI Scan Image. (B) Cropping Random Section of Liver. (C) Histogram of Cropped Liver Section. (D) Result of Histogram-Based Segmentation. (E) Liver Boundary in MRI. (F) Ground Truth Image.

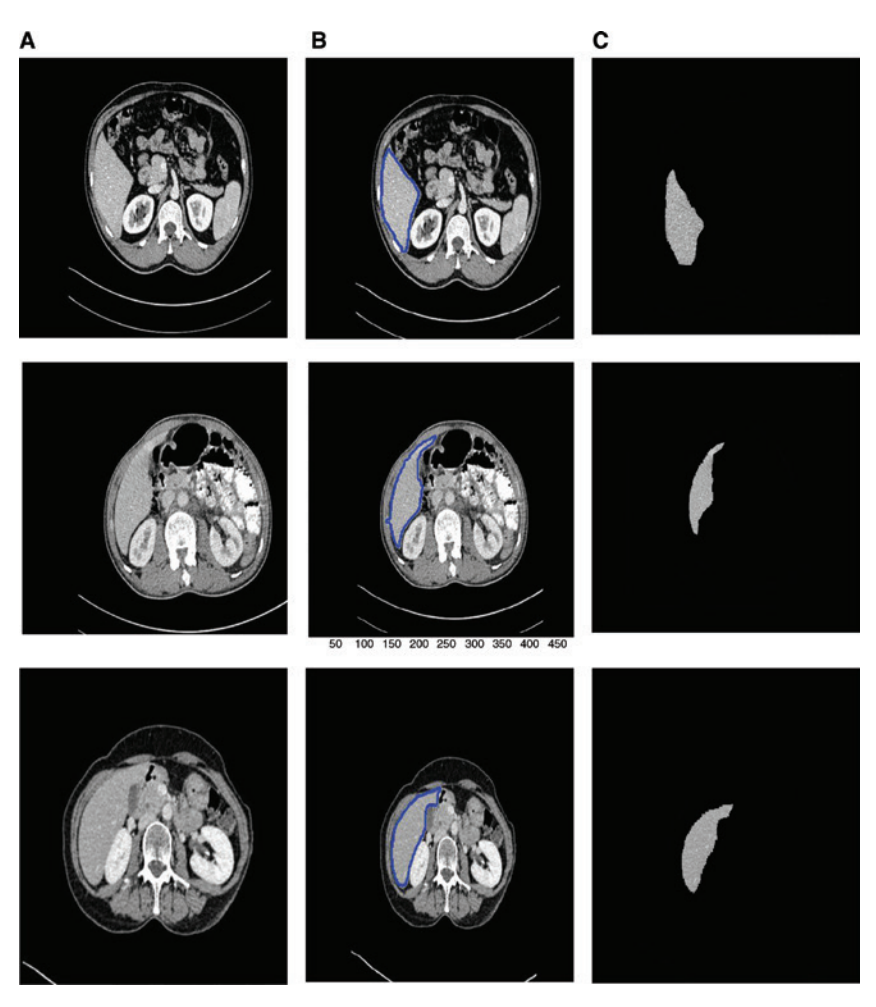


Figure 4: Experimental Results of Proposed Method for CT Scan Images. (A) Original CT scan image; (B) CT scan with liver boundary; (C) ground truth image.

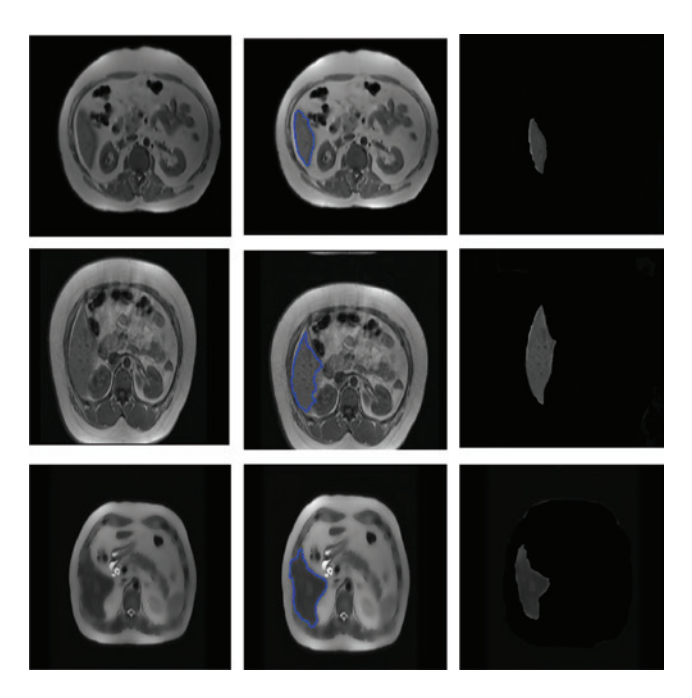


Figure 5: Experimental Results of Proposed Method for MRI Scan Images.

8 Comparison with Existing Methods and Discussions

In this section, the performance of the proposed method is compared with the C-V model [1], with specifications: $\mu = 0.1$, number of iterations = 170, and initial contour position = [330, 310; 340, 330].

The LSE (level set evolution) model [7] demonstrated the segmentation process. The analysis was performed on the CT scan image with the following specifications: $\mu = 1.0$, $\varepsilon = 1.0$, time step = 0.1, $\varsigma = 4$, initial contour position = [160, 220; 190, 240], number of iterations = 10.

The RSF (region-scalable fitting] model [6] demonstrated the segmentation process, and the analysis was performed on the CT scan image with the following specifications: $\zeta = 3.0$, $\varepsilon = 1.0$, $\mu = 1.0$, time step = 0.1, $\lambda 1 = 1.0$, $\lambda 2 = 1.0$, number of iterations = 25, initial contour position = [160, 200; 180, 200].

The comparison results of the proposed method and existing methods are shown in Figure 6. The original CT scan image and MRI scan image are shown in column A; the results of the original C-V model on the CT

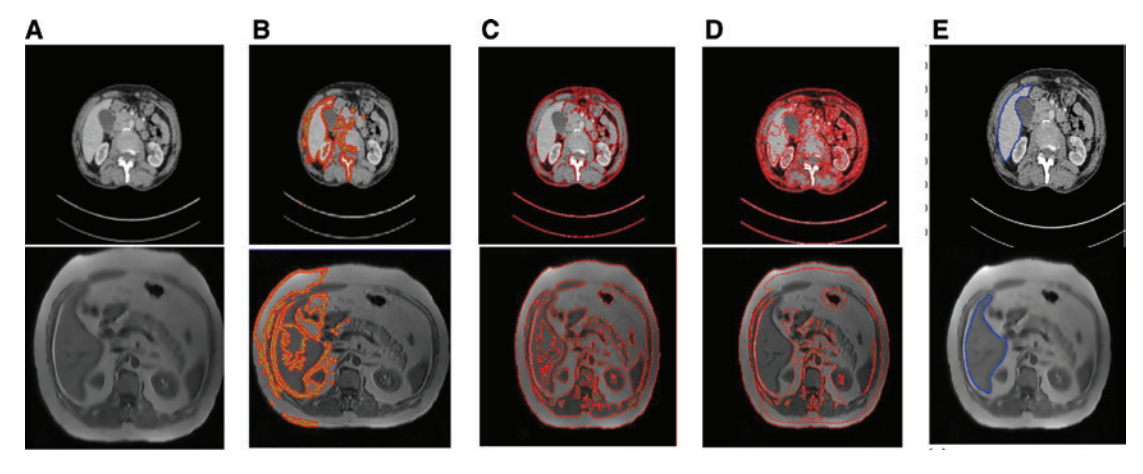


Figure 6: Comparison Result of Proposed Method with Existing Method.

Column (A) Original CT Scan and MRI Scan. (B) Result of C-V Model on CT Scan and MRI Scan. (C) Result of LSE Model on CT Scan and MRI Scan. (D) Result of RSF Model on CT and MRI Scan Image. (E) Result of Proposed Model.

scan and MRI scan images are shown in column B; the results of the LSE model are shown in column C; the results of the RSF model are shown in column D; the results of the proposed model are shown in column E.

The proposed algorithm, the original C–V model, the LSE model, and the RSF model were tested for 50 images of the CT scan and 50 MRI scan images. The VOE (in %) for the proposed method and existing method were calculated for the 50 CT scan images and 50 MRI scan images and are shown in Figures 7 and 8, respectively. The RVD (in %) for the proposed method and existing method were calculated for the 50 CT scan images and 50 MRI scan images and are shown in Figures 9 and 10, respectively. The ASSD (in mm) for the proposed method and existing method were calculated for the 50 CT scan images and 50 MRI scan images and are shown in Figures 11 and 12, respectively. The MSSD (in mm) for the proposed method and existing method were calculated for the 50 CT scan images and 50 MRI scan images and are shown in Figures 13 and 14, respectively. Tables 1 and 2 represent the average VOE in %, RVD in %, ASSD in mm, and MSSD in mm using the CT scan and MRI scan images, respectively.

The liver and its neighboring organs have the same intensity level distribution, due to more noise and blurry edges. All three existing algorithms have limitations, resulting in an inaccurate detection of the exact liver section. The proposed methodology fully exploits the intensity distribution information by cropping the random section of the liver and its segmentation resulting in a successful separation of the liver image from its neighboring organs.

In the C–V, LSE, and RSF models, it is necessary to identify the initial contour and number of iterations manually. These parameters will affect the segmentation results. In the proposed method, there is no need to identify the number of iterations and initial contour. Once the complete liver boundary is detected, the results will be displayed on the computer screen. The initial contour is identified without user intervention.

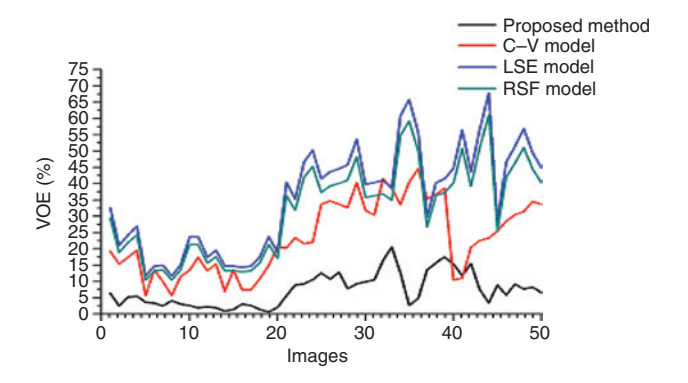


Figure 7: Comparison of Results Using VOE for CT Scan Images.

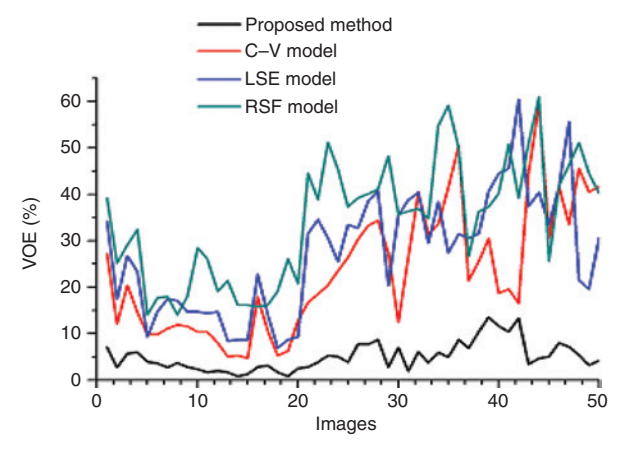


Figure 8: Comparison of Results Using VOE for MRI Scan Images.

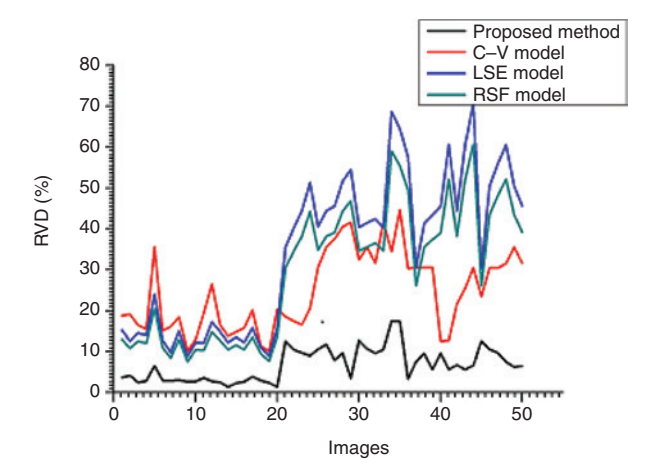


Figure 9: Comparison of Results Using RVD for CT Scan Images.

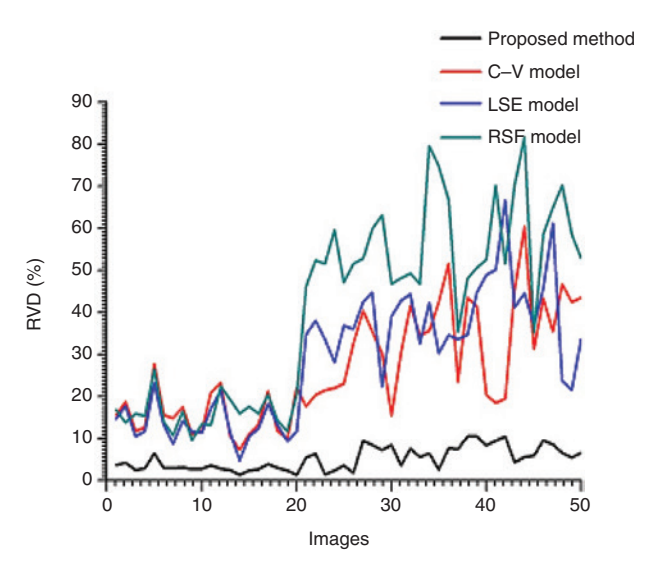


Figure 10: Comparison of Results Using RVD for MRI Scan Images.

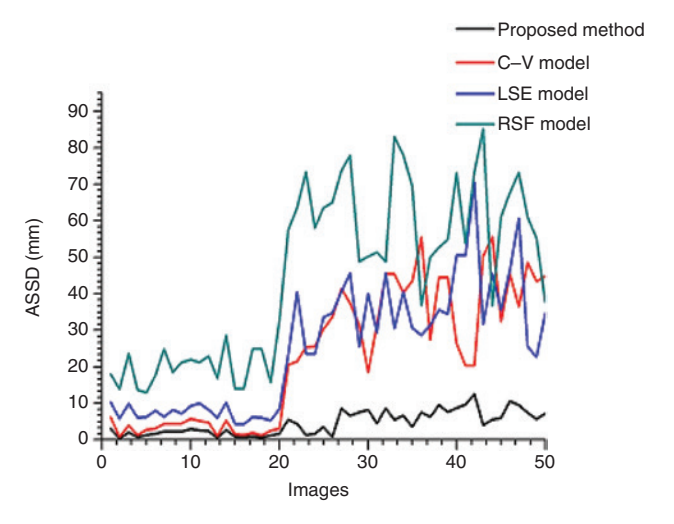


Figure 11: Comparison of Results Using ASSD for CT Scan Images.

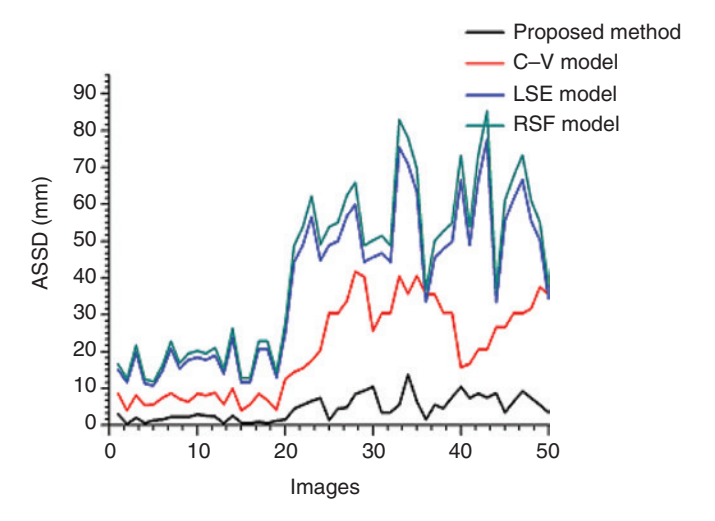


Figure 12: Comparison of Results Using ASSD for MRI Scan Images.

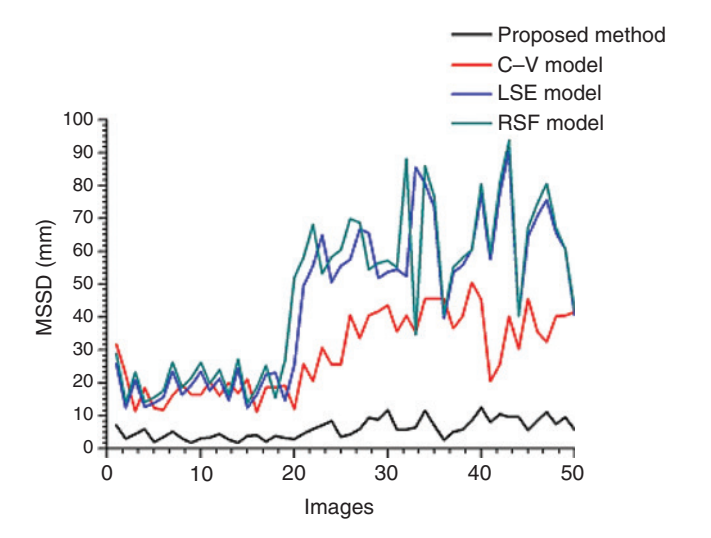


Figure 13: Comparison of Results Using MSSD for CT Scan Images.

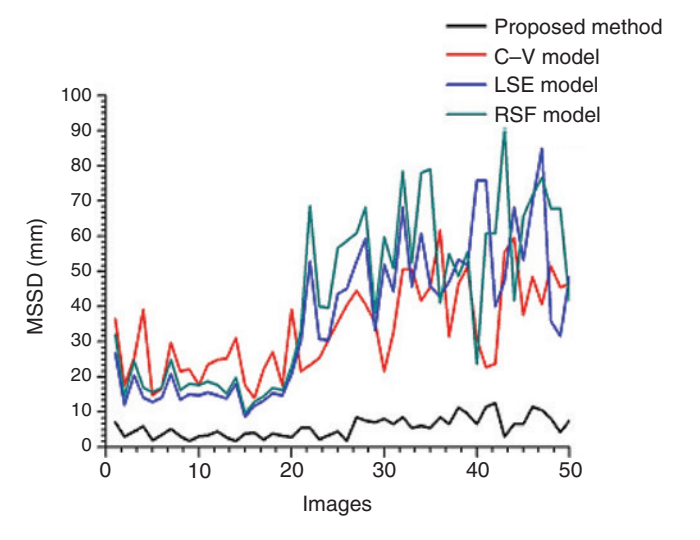


Figure 14: Comparison of Results Using MSSD for MRI Scan Images.

Table 1: Average VOE, RVD, ASSD, and MSSD for the Proposed Models and Existing Algorithm Using CT Scan.

	VOE (%)	RVD (%)	ASSD (mm)	MSSD (mm)
Proposed model	5	5.1	4.6	4.5
C-V model	23.6	26.6	34.2	27.1
LSE model	27.4	28.7	25.1	28
RSF model	34.4	40.4	44.7	48.4

Table 2: Average VOE, RVD, ASSD, and MSSD for the Proposed Models and Existing Algorithm Using MRI Scan.

	VOE (%)	RVD (%)	ASSD (mm)	MSSD (mm)
Proposed model	7.4	6.8	4.7	4.9
C-V model	23.3	24.7	20.3	21.8
LSE model	35.5	34.5	38.5	43.3
RSF model	32	29.7	42.4	50.7

9 Conclusions

This paper designs the universal liver segmentation method, which can be implemented on MRI images as well as on CT images. The histogram-based threshold segmentation is used to separate the liver from its neighboring organs, and the improved C-V model is utilized to find the periphery of the liver. The novel approach is designed to detect the initial contour automatically, which evolves outward until it reaches the liver boundary. This can be used in finding the area and volume of the liver, which is required for physicians for liver disease diagnoses and liver transplantation. This method can be used for other modalities without any change as well as to find the outline of other organs.

Acknowledgement: The authors acknowledge the support of M/S Hubli Scan Center, Hubli, Karnataka, India, and the doctors for their suggestions and certifications of results. The authors are thankful to the management and authorities of the JSS Academy of Technical Education, Bengaluru, Karnataka, India, and Sapthagiri College of Engineering, Bengaluru, Karnataka, India.

Bibliography

- [1] T. Chan and L. A. Vese, Active contours without edges, in: IEEE Transactions On Image Processing, IEEE Inc., New York, 2001.
- [2] Y. Chen, Z. Wang and W. Zhao, Liver segmentation in CT images using Chan-Vese model, in: The 1st International Conference on Information Science and Engineering (ICISE2009), Nanjing, China, 2009, 978-0-7695-3887-7/09.
- [3] X. Ding, X. Geng, C. Jiang, F. Tian, X. Yan, H. Qi, L. Zhang and Y. Zheng, Fast automated liver delineation from computational tomography angiography, Procedia Comput. Sci. 90 (2016), 87-92.
- [4] Z. Gang, H.-N. Wang and Y.-L. Li, A tree-like multiphase level set algorithm for image segmentation based on the Chan-Vese model, Dianzi Xuebao (Acta Electronica Sinica) 34.8 (2006), 1508–1512.
- [5] T. Heimann, B. van Ginneken, M. A. Styner, Y. Arzhaeva, V. Aurich, C. Bauer, A. Beck, C. Becker, R. Beichel, G. Bekes, F. Bello, G. Binnig, H. Bischof, A. Bornik, P. Cashman, Y. Chi, A. Cordova, B. M. Dawant, M. Fidrich, J. D. Furst, D. Furukawa and L. Grena, Comparison and evaluation of methods for liver segmentation from CT datasets, IEEE Trans. Med. Imaging 28 (2009), 1251-1265.
- [6] C. Li, C.-Y. Kao, J. C. Gore and Z. Ding, Minimization of region-scalable fitting energy for image segmentation, IEEE Trans. Image Process. 17 (2008), 1940-1949.
- [7] C. Li, R. Huang, Z. Ding, J. C. Gatenby, D. N. Metaxas and J. C. Gore, A level set method for image segmentation in the presence of intensity inhomogeneities with application to MRI, IEEE Trans. Image Process. 20 (2011), 2007–2016.
- [8] G. Li, X. Chen, F. Shi, W. Zhu and J. Tian, Automatic liver segmentation based on shape constraints and deformable graph cut in CT images, IEEE Trans. Image Process 24 (2015), 5315-5329.

- [9] F. Lu, F. Wu, P. Hu, Z. Peng and D. Kong, Automatic 3D liver location and segmentation via convolution neural network and graph cut, Int. J. Comput. Assist. Radiol. Surg. 12.2 (2017), 171-182.
- [10] J. Min, M. Powell and K. W. Bowyer, Automated performance evaluation of range image segmentation algorithms, IEEE Trans. Syst. Man Cybern., Part B (Cybernetics) 34.1 (2004), 263-271.
- [11] M. Moghbel, S. Mashohor, R. Mahmud and M. I. B. Saripan, Automatic liver segmentation on computed tomography using random walkers for treatment planning, EXCLI J. 15 (2016), 500.
- [12] D. Mumford and J. Shah, Optimal approximation by piecewise smooth functions and associated variational problems, Commun. Pure Appl. Math. 42 (1989), 577-685.
- [13] J. Peng, P. Hu, F. Lu, Z. Peng, D. Kong and H. Zhang, 3D liver segmentation using multiple region appearances and graph cuts, Med. Phys. 42 (2015), 6840-6852.
- [14] C. Platero and M. C. Tobar, A multiatlas segmentation using graph cuts with applications to liver segmentation in CT scans, Comput. Math. Methods Med. 2014 (2014), 16 Article ID 182909.
- [15] S. Pramod Kumar and M. V. Latte, Fully automated segmentation of lung parenchyma using break and repair strategy, J. Intell. Syst. De Gruyter 28 (2019), 275-289.
- [16] D. V. Sahani and S. P. Kalva, Imaging the liver, *Oncologist* 9 (2004), 385–387.
- [17] S. D. Salman Al-Shaikhli, M. Y. Yang and B. Rosenhahn, 3D automatic liver segmentation using feature-constrained Mahalanobis distance in CT images, Biomed. Tech. 61 (2015), 401-412.
- [18] S. Siri and M. V. Latte, A novel approach to extract exact liver image boundary from abdominal CT scan using neutrosophic set and fast marching method, J. Intell. Syst. 28 (2019) 517-532.
- [19] X. Song, M. Cheng, B. Wang and S. Huang, Automatic liver segmentation from CT images using adaptive fast marching method, in: Seventh International Conference on Image and Graphics, Qingdao, China, 2013, 978-0-7695-5050-3-2013 IEEE DOI-10.1109/ICIG.2013.181.
- [20] W. Wu, Z. Zhou, S. Wu and Y. Zhang, Automatic liver segmentation on volumetric CT images using supervoxel-based graph cuts, Comput. Math. Methods Med. 2016 (2016), 1-14.
- [21] J. Zhao, X. Zhang, W. Huang, F. Shao and Y. Xu, An improved Chan-Vese model without reinitialization for medical image segmentation, in: 2010 3rd International Congress on Image and Signal Processing, Yantai, China, 2010.
- [22] Y. Zheng, D. Ai, P. Zhang, Y. Gao, L. Xia, S. Du, X. Sang and J. Yang, Feature learning based random walk for liver segmentation, PLoS One 11 (2016), 1-17.